

To the Graduate Council:

I am submitting herewith a thesis written by Krishna Thapa entitled "Correction to Luminosity Measurement for the Pixel Luminosity Telescope at CMS." I have examined the final paper copy of this thesis for form and content and recommend that it be accepted in partial fulfillment of the requirements for the degree of Master of Science, with a major in High Energy Physics.

Stefan M. Spanier, Major Professor

We have read this thesis
and recommend its acceptance:

Dr. Stefan Spanier

Dr. Marinne Breining

Dr. Thomas Handler

Accepted for the Council:

Carolyn R. Hodges

Vice Provost and Dean of the Graduate School

To the Graduate Council:

I am submitting herewith a thesis written by Krishna Thapa entitled "Correction to Luminosity Measurement for the Pixel Luminosity Telescope at CMS." I have examined the final electronic copy of this thesis for form and content and recommend that it be accepted in partial fulfillment of the requirements for the degree of Master of Science, with a major in High Energy Physics.

Stefan M. Spanier, Major Professor

We have read this thesis
and recommend its acceptance:

Dr. Stefan Spanier

Dr. Marinne Breining

Dr. Thomas Handler

Accepted for the Council:

Carolyn R. Hodges

Vice Provost and Dean of the Graduate School

(Original signatures are on file with official student records.)

Correction to Luminosity Measurement for the Pixel Luminosity Telescope at CMS

A Thesis Presented for

The Master of Science

Degree

The University of Tennessee, Knoxville

Krishna Thapa

December 2016

© by Krishna Thapa, 2016

All Rights Reserved.

dedication...

Acknowledgements

I would like to thank...

Some quotation...

Abstract

The search for and detailed study of new particles and forces with the Compact Muon Solenoid (CMS) detector at the Large Hadron Collider (LHC) of CERN is fundamentally dependent on the precise measurement of the rate at which proton-proton collisions produce any particles, the so-called luminosity. Therefore, a new detector, the Pixel Luminosity Telescope (PLT), dedicated to measure the luminosity at high precision was added to the CMS experiment in 2015. It measures the inclusive charged particle production from each collision of proton bunches in the LHC. The instrument provides measurements of particle trajectories which allows to distinguish particles originating from proton proton collisions and other sources that accidentally are created as luminosity contribution. Methods were developed to calculate the corrections to the luminosity measurement of the PLT.

Contents

List of Tables	ix
List of Figures	x
1 Introduction	1
2 Physics Background	3
2.1 Standard Model of Particle Physics	3
2.2 Luminosity	5
2.3 Luminosity Calibration	10
2.4 Luminosity Measurement	12
3 Experimental Setup	15
3.1 Large Hadron Collider	15
3.1.1 Filling Scheme	17
3.1.2 LHC Operations in 2015 and 2016	17
3.2 CMS	19
3.3 Pixel Luminosity Telescope	24
3.3.1 Triple coincidence measurement	28
3.3.2 Zero Counting Algorithm	29
3.3.3 Van der Meer Scan Calibration	29
4 Operations of PLT	34

5 Event Reconstruction	35
6 Luminosity Correction	36
Bibliography	37
A Summary of Equations	42
A.1 Cartesian	42
A.2 Cylindrical	42
Vita	43

List of Tables

2.1	Rough order of the interaction strengths and the mediators for interactions.	4
2.2	LHC beam parameters relevant for the peak luminosity Bailey and Collier (2004)	8

List of Figures

2.1	The standard model of particle physics with three generations of matter fermions, gauge bosons and a Higgs boson. Figure taken from User:MissMJ et al. (2014)	4
2.2	Two colliding proton beam bunches with idealized shape	6
2.3	The cross sections and expected production rates at the LHC and the Tevatron.	7
2.4	Two proton bunches with more realistic profile colliding at an angle .	9
3.1	Layout of the CERN accelerator complex with four LHC experiments CMS, ALICE, ATLAS, and LHCb Lefvre (2008).	16
3.2	Schematic of the Bunch Disposition around an LHC Ring for the 25 ns Filling Scheme Bailey and Collier (2004). 'b' and 'e' indicate beam position with or without beam.	18
3.3	Mean number of interactions per bunch crossing, 2012.	19
3.4	CMS Coordinate System with positive x towards the center of the ring	20
3.5	Relationship between polar angle and pseudorapidity.	21
3.6	Delivered Luminosity versus time for several years of data taking of pp collisions with the CMS detector CMS Collaboration (2016).	22
3.7	CMS Detector Sakuma (2016).	23
3.8	PLT Module.	24
3.9	PLT modules at forward direction(left) and backward direction (right) both located at 171 cm from the interaction point.	25

3.10 A schematic of the control and readout logic of Pixel Luminosity Telescope.	25
3.11 Bunches triggered via random trigger setup for \sim 10 lumi sections from Fill 5151 (2016) with 1579 BX cycling every 3 orbits	27
3.12 Tracks which make through all 3 planes with a mask of 4mm x 4mm	28
3.13 Per channel average coincidence count for 1 nibble sample from Fill 4444 (2015)	30
3.14 Comparison of luminosity measured via LHC beam parameters and Pixel Luminosity Detector for the CMS experiment, Fill 5253.	32
3.15 Double Gaussian fit to PLT track rate as a function of beam separation, for bunch 1011 during the first separation/crossing VdM scan in X and Y.	33

Chapter 1

Introduction

The quest for understanding the fundamental nature of the physical world around us has taken us from studying tangible objects in our proximity to studying celestial bodies millions of light years away. The nature of physical world, either at large or small scale, is governed by a common set of laws that we seek to understand. To that end, the experiments in elementary particle physics probe interactions between sub atomic particles to probe the fundamental laws of nature. The standard model [ref] of particle physics is a well tested theory that lays out the important parameters for the interaction between particles. Prediction of the existence of the top quark (1995), neutrino (2000), and Higgs (2012) have been confirmed experimentally. This model attempts to describe the electromagnetic, weak, and strong nuclear interactions among subatomic particles.

Despite it's many successes, standard model is not a complete theory. For example, gravitational interactions, the matter-antimatter asymmetry in the universe among others, is not predicted in agreement with observations by the current model. There are extensions to the SM that predict the existence of new generations of particles and forces [...] at higher energies accessible with accelerators until recently.

Some of these ideas can be tested experimentally at the Large Hadron Collider (LHC) at CERN that collides protons at unprecedeted high beam energy and

intensities to produce particles of higher masses and measure rare particle reactions. At any time the precise knowledge of the rate at which proton proton collision produce any particles, the so called luminosity, is crucial to obtain absolute production rate of the new signals that are compared to theoretical predictions, and to accurately predict the production of fake signals that need to be subtracted.

The luminosity eventually sets limit on the confidence of our physics findings. My thesis work concerns systematic studies of the PLT and the determination of background to the luminosity measurement. This thesis describes the measurement of the luminosity delivered to the CMS's PLT detector at the LHC in proton proton (pp) collisions at a center-of-mass energy 13 TeV during the 2015-2016 run period. This thesis is structured the following: Chapter 2 provides a brief overview of the standard model of particle physics and the concept of luminosity. Chapter 3 describes the experimental setup for the PLT and the method used for calibration.

CMS installed the Pixel Luminosity Telescope (PLT) in 2015; software for analyzing the machine conditions and measurement data had to be built. Chapter 4 provides an overview of operational work done as part of the thesis. Charged particle reconstruction, likelihood fits to extract signal and background contributions and corrections to the published luminosity values are discussed in chapter 5 and 6.

Chapter 2

Physics Background

2.1 Standard Model of Particle Physics

The standard model (SM) of particle physics describes the interaction between elementary particles through electromagnetic, weak, and strong forces via the exchange of force mediator particles. This model unifies theories on electromagnetic and weak interactions as published in 1961 [ref Sheldon Glashow], with the addition of Higgs mechanism in 1967 by [Steven Weinberg and Abdus Salam]. This theory successfully explained the experimental observations in the past, as shown in Figure ??, and continues to provide avenues to probe the theory further.

According to the SM, matter consists of particles of spin 1/2 known as fermions each of which has its own antiparticle of opposite spin. These particles are treated as excitations of fields, and the forces are treated as interactions between these excitations. The interactions happen via exchange of various vector bosons, which are the particles with spin 1. There are two groups of fermions: that interact electromagnetically and weakly. The Leptons—electron, muon, tau, and their partner neutrinos only experience the electroweak force. The quarks—up, down, strange, charm, bottom, top experience both the electroweak force and the strong force. Higgs boson, with spin 0, generates mass of particles. As the unification in the SM a priori

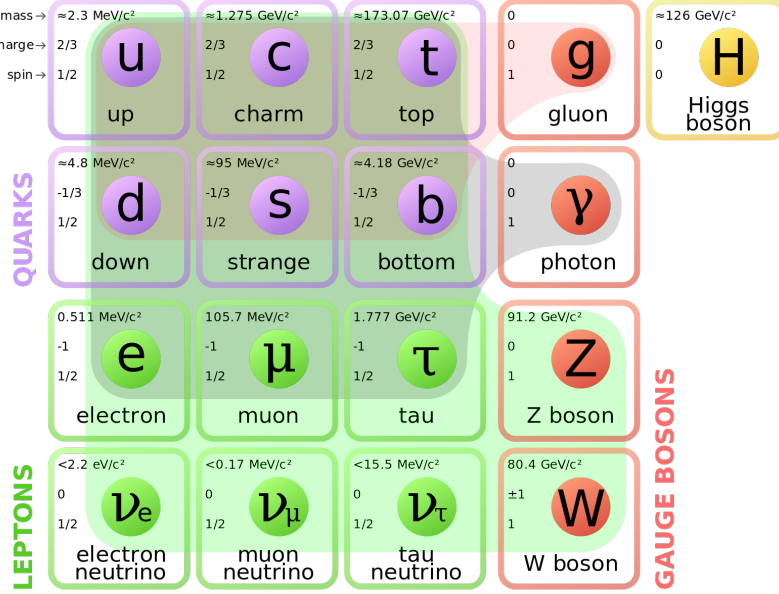


Figure 2.1: The standard model of particle physics with three generations of matter fermions, gauge bosons and a Higgs boson. Figure taken from User:MissMJ et al. (2014)

Interaction	Strength	Mediator
Strong	10	Gluon
Electromagnetic	10^{-2}	Photon
Weak	10^{-3}	W and Z Bosons
Gravitation	10^{-42}	Graviton

Table 2.1: Rough order of the interaction strengths and the mediators for interactions.

only is valid with massless particles, Higgs mechanism describes the process by which particles require mass.

The particle content of the SM is summarized in Figure 2.1. Protons and neutrons that make up most of the matter around us are composed of quarks.

Despite its successes in describing particle interactions at energies accessible with particle accelerators, the SM is not a complete theory of the universe. This is among the strongest reason to search for physics beyond the SM. During future data-taking

periods LHC hopes to push our understanding forward by observing new generations of particles and particle interaction rates that deviate from SM predictions.

2.2 Luminosity

The quantity that measures the ability of a particle collider to produce the required number of interactions is called the luminosity \mathcal{L} . Its precise knowledge is important since for many cross-sections measurements the uncertainty factor on the luminosity dominates the final result. Luminosity is the proportionality factor between the number of events per second $R(t)$ at a given time t and its production cross-section σ_P for a process:

$$R(t) = \mathcal{L}(t) \cdot \sigma_P \quad (2.1)$$

This defines the so-called instantaneous luminosity commonly measured in units of $\text{cm}^{-2} \text{s}^{-1}$. Typically running conditions vary with time t . Therefore, the luminosity of a collider also has a time dependence that needs to be carefully measured to arrive at integrated luminosity for a given data taking period which is given as:

$$\mathcal{L}_{int} = \int \mathcal{L}(t) dt \quad (2.2)$$

and measured in units of b^{-1} ^{*}. The delivered integrated luminosity, which refers to the integrated luminosity which the machine has delivered to an experiment, and recorded integrated luminosity, which refers to the amount of data that has actually been stored to disk by the experiments typically differ and hence an independent measurement by the experiment is necessary.

As \mathcal{L} is process-independent it is possible to measure the luminosity with any process whose cross-section is known. For a precise luminosity determination, however, it is essential that the process has precise theoretical predictions and at

^{*}1 barn = 10^{-28} cm^2

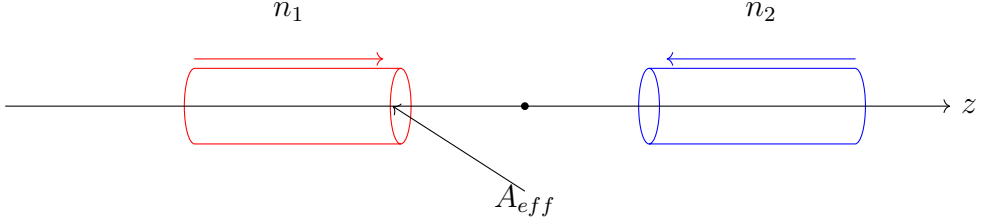


Figure 2.2: Two colliding proton beam bunches with idealized shape

the same time that its rate can be accurately measured, i.e. enough signal events are produced and reconstructed in a limited time interval. The production of Z^0 bosons ($pp \rightarrow Z^0 X$) that decay into leptons, particularly muons ($Z^0 \rightarrow \mu^+ \mu^-$), is such a "standard candle process", because the leptons can be well identified and theoretical prediction of the cross section has only a few percent relative uncertainty. The cross-section of Z^0 production is large enough and there are almost no fake signals.

The instantaneous luminosity can be extracted from certain beam parameters. A simplified case for a head-on collision of two bunches is shown in Figure 2.2. The luminosity can be expressed in terms of geometry and the number of particles in each of the two colliding beam bunches $n_{1(2)}$:

$$\mathcal{L} = \frac{n_1 n_2 f}{A_{eff}}, \quad (2.3)$$

with f the collision frequency. Beam parameters for the LHC are listed in Table 2.2. Of the possible 3564 bunches only $n_b = 2808$ are filled reducing the peak luminosity accordingly. The beam current $I_{1(2)}$ is given in terms of the charge of the beam particle e and the collision frequency f as $I_i = e_i f n_i$. Hence, one obtains

$$\mathcal{L}_{int} = \frac{I_1 I_2}{e^2 f A_{eff}} \quad (2.4)$$

With a nominal instantaneous luminosity of $\mathcal{L} = 10^{34} \text{ cm}^{-2} \text{s}^{-1}$ ($= 10 \text{ nb}^{-1} \text{s}^{-1}$) and a Higgs production cross section of $\sigma \simeq 0.1 \text{ nb}$ one expects about 1 Higgs per second. Figure 2.3 shows the cross sections for several processes at a 10 times lower nominal luminosity that has been achieved so far with the LHC. At this luminosity also about

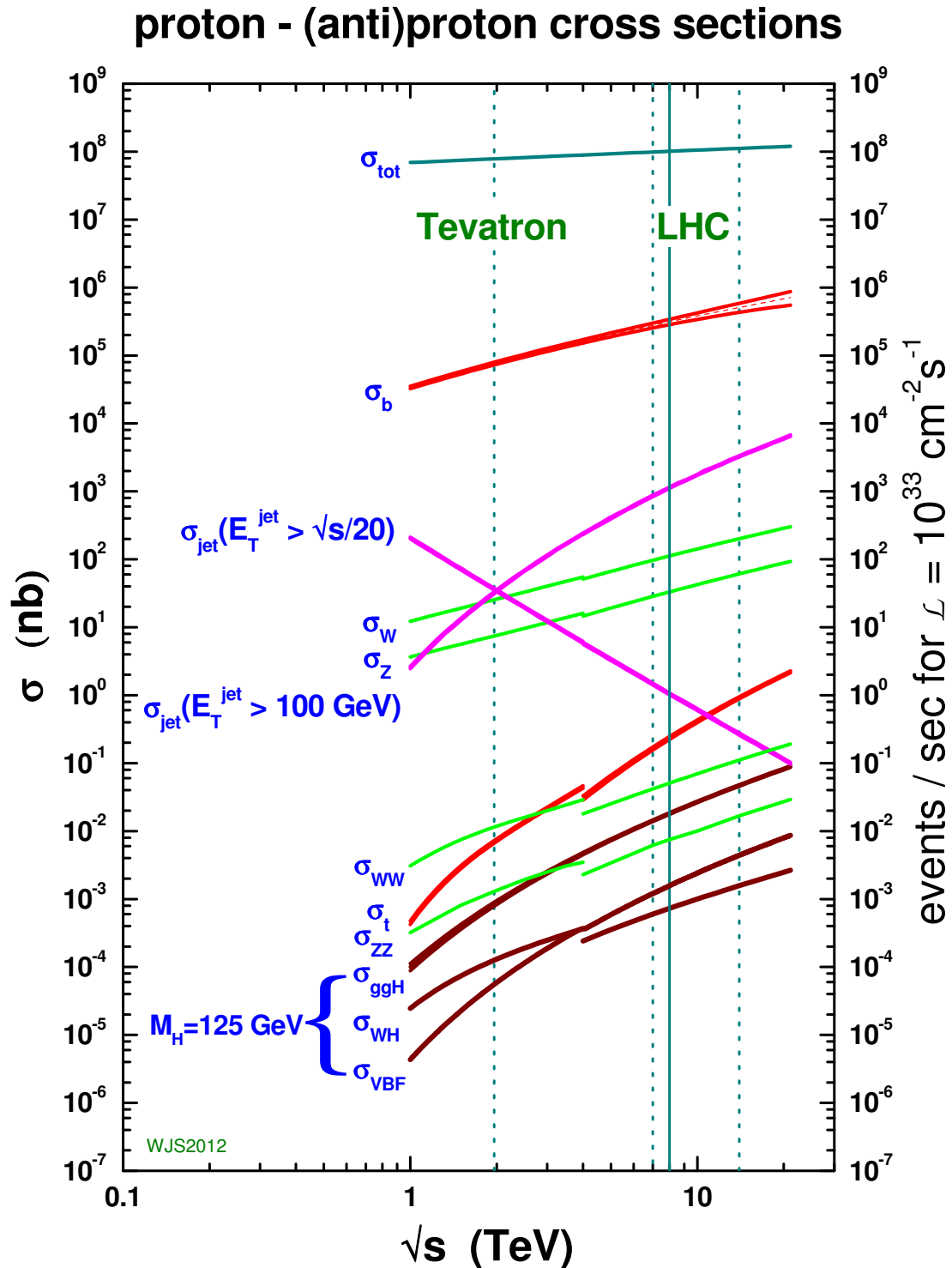


Figure 2.3: The cross sections and expected production rates at the LHC and the Tevatron.

100 Z^0 particles are produced per second. Only 3.4 % of Z^0 's decay into a muon pair resulting in about 3 Z^0 particles per second that are potentially detected and reconstructed with CMS.

Beam Parameter	Unit	Value
Proton Energy	[GeV]	6500
Stored energy per beam	[MJ]	363
Number of particles per bunch n_i		1.15×10^{11}
Number of bunches n_b		2808
Bunch collision frequency f	MHz	40
Circulating beam current	[A]	0.584
Transverse beam size ($\sigma_{x,y}$)	μm	16.7
RMS bunch length (σ_z)	cm	7.55
Geometric luminosity reduction factor F		0.836
Peak luminosity in IP1 and IP5	[$cm^{-2}sec^{-1}$]	10^{34}

Table 2.2: LHC beam parameters relevant for the peak luminosity [Bailey and Collier \(2004\)](#)

Assuming that the transverse profile of the two bunches distribute identically and that the profiles do not change along the bunch a good approximation is a Gaussian profile for the beam transverse distribution in x and y , each characterized with a standard deviation σ_x and σ_y , respectively. In this case $A_{eff} = 4\pi\sigma_x\sigma_y$. It implies that the profiles in x and y direction are not correlated.

The two beams at the LHC cross each other under an angle of $\theta_C = 285\mu$ rad to direct the beams after collision into their respective vacuum pipe and to avoid multiple unwanted interactions. Figure 2.4 shows a schematic illustration of the beam crossing. It also shows a change in the profile along the beam width. The correct evaluation of the effective beam size is obtained from an overlap integral of beam density distribution functions in all three coordinates [Herr and Muratori \(2003\)](#). For small angles, Gaussian profiles and $\sigma_x \simeq \sigma_y$ in good approximation this results in the so called geometric luminosity reduction factor F, given as

$$F = \left(\sqrt{1 + \left(\frac{\theta_c \sigma_z}{2\sigma^*} \right)^2} \right)^{-1} \quad (2.5)$$

that multiplies eq. 2.3.

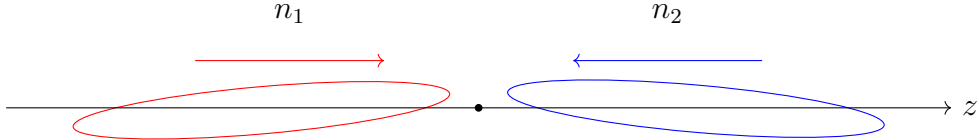


Figure 2.4: Two proton bunches with more realistic profile colliding at an angle

In practice, however, there are complications: beams do not factorize as the profile changes over the length of the bunch and bunches do not collide exactly head-on but with offsets. Imperfections in the beam steering lead to widening of the beam profile and therefore a reduced luminosity. So far also a uniform population of the beam bunches is assumed while in reality the actual fill pattern can vary. The LHC provides measurements of beam currents and beam profiles along the LHC accelerator but not in the vicinity of the interaction points. Furthermore, the beam parameters and conditions change over the time period of a LHC fill. To arrive at the best time-integrated luminosity the time integral has to be taken over time intervals short enough to measure significant variations and exclude dead times. Typically the beam intensity decays exponentially with time resulting in a similar reduction in the instantaneous luminosity. The effective mean lifetime of the luminosity is further reduced by the increase of the transverse and longitudinal beam size over time. To reduce uncertainties due to extrapolation from beam parameter measurements the CMS experiment has to measure the relative luminosity with dedicated detectors and calibrate them with standard candle processes or dedicated calibration runs of the LHC.

2.3 Luminosity Calibration

One can obtain the absolute luminosity directly from beam parameters according to Eq. 2.2, without the a priori knowledge of any physics cross section. The revolution frequency f is well known and the number of particles $n_{1(2)}$ can be measured by dedicated beam charge monitors. In contrast, the transverse area of beam overlap A_{eff} is difficult to determine. Different monitors such as wire scanners or synchrotron light monitors can sample the beam profile but not close to the collision points and extrapolations lack precision. In the year 1968 Simon van der Meer proposed a method to measure A_{eff} [Van Der Meer \(1968\)](#), now known as van der Meer- (vdm-) or beam separation-scan.

Simon van der Meer proposed that it is possible to measure the profile of colliding beams by observing the counting rate R in a particle counting system, while scanning the two beams vertically across each other. One of the two beams is displaced vertically with respect to the other one, and the counting rate in the monitor is plotted versus displacement. A bell-shaped curve will result with its maximum at zero displacement, then independent of beam shape A_{eff} is equal to the area under this curve, divided by the ordinate for zero displacement [Van Der Meer \(1968\)](#). At the LHC the measured counting rate depends on both horizontal and vertical beam sizes. The main assumption is that the density distributions of particles in bunches can be factorized, and two scans along the transverse planes are sufficient. If one assumes that the beam density functions are uncorrelated one can write for the counting rate R as function of displacement in x and y , δx and δy , respectively:

$$R(\delta x; \delta y) = R_x(\delta x)R_y(\delta y) \quad (2.6)$$

By scanning the two transverse planes, one obtains a direct measurement of the transverse effective beam sizes and therefore of the effective area A_{eff} :

$$A_{eff} = \frac{\int R_x(\delta x) d\delta x}{R_x(0)} \frac{\int R_y(\delta y) d\delta y}{R_y(0)} \quad (2.7)$$

The convoluted transverse width per scan direction of the two beams can be written as:

$$\Sigma_x = \sqrt{\sigma_{1x}^2 + \sigma_{2x}^2} = \frac{1}{\sqrt{2\pi}} \frac{\int R_x(\delta x) d\delta x}{R_x(0)} \quad (2.8)$$

and the same expression for Σ_y in y direction. The luminosity Eq. 2.2 becomes:

$$\mathcal{L}_{int} = \frac{n_1 n_2 f}{2\pi \Sigma_x \Sigma_y} \quad (2.9)$$

In case of a crossing angle, the vdM scan measures directly the correct effective beam size, including the effect of a crossing-angle for scans performed exactly in the crossing plane White et al. (2010) Figure 3.15 shows the rate of particle tracks as measured with the PLT versus the separation in the beam in x direction. The data points have been fit to a Gaussian function. A refined fit uses two Gaussian functions to achieve an improved description of the tails in the distribution.

The CMS collaboration uses the PLT detector to measure and monitor the relative luminosity. Once calibrated, one can extrapolate the absolute luminosity measurement of the vdM scan to any other luminosity scenario. With R_{inel} to be the rate of inelastic pp events, σ_{inel} the pp inelastic cross-section, f the revolution frequency of the bunches, and μ the average number of pp -collisions per bunch-crossing:

$$\mathcal{L}_{int} = \frac{R_{inel}}{\sigma_{inel}} = \frac{\mu f}{\sigma_{inel}} \quad (2.10)$$

The PLT detector with limited acceptance times detection efficiency ω will only see a subset of the events:

$$\mathcal{L}_{int} = \frac{\omega \mu f}{\omega \sigma_{inel}} = \frac{\mu_{vis} f}{\sigma_{vis}} \quad (2.11)$$

The index vis stands for visible value. Hence, the μ_{vis} can be measured and $\sigma_{\text{vis}} = \sigma_{\text{inel}}$ is practically the calibration constant to obtain the absolute luminosity. In general, this equation is valid only in the case of a linear response of the detector with respect to μ . Otherwise corrections for the non-linearity must be taken into account.

2.4 Luminosity Measurement

The PLT detector consists of two symmetric detector arms placed on each side of the CMS interaction point (IP5). Each side is further divided into eight telescopes with each treated as separate readout channel. Particles passing through one of these telescopes are counted as hit if their charge signals in all three detectors of the telescope are simultaneously above threshold (Fast-OR). A bunch crossing is counted as an event when there is at least one hit. The typical rate μ per bunch crossing in 2015 was 1 hit on each side respective a detector occupancy of about 0.15/BCX. Particles not originating from bunch collisions but rather collision in the beam gas and with beam halo particles result in a miscount of the luminosity and are subtracted statistically after a detailed analysis of their relative contribution. The relative contribution from such background was at most 7% in 2015. The analysis is described in detail in [Lujan et al. \(2016\)](#). The luminosity is determined by event-counting. A disadvantage of this method is that one is limited to measure either any hit or no-hit event which at high μ results in the event probability approaching one. Then every bunch crossing will be counted as an event and the method does not work anymore (is saturated).

One can derive the probability for multi-interaction events making the assumption that the number of pp interactions during a bunch crossing follows a Poisson statistics the following:

$$P_\mu(n) = \sum_{n=0}^{\infty} \frac{\mu^n e^{-\mu}}{n!} \quad (2.12)$$

where $P_\mu(n)$ is the probability to have n interactions in a bunch crossing when the average number of interactions is μ . Furthermore, the probability to detect a single interaction ω (efficiency \times acceptance of the PLT Fast-OR) is assumed not to change when several events in the same bunch crossing happen. This effect is expected to be negligible for occupancies of significantly less than 1 per bunch crossing per channel. The probability for *not* detecting a bunch crossing that has n interactions is given as:

$$P_0(n) = (1 - \omega)^n \quad (2.13)$$

With n distributed according to a Poissonian the probability to measure μ interactions when the average number is zero is:

$$P_0(\mu) = \sum_{n=0}^{\infty} (1 - \omega)^n \cdot P_\mu(n) \quad (2.14)$$

and using the expansion one obtains:

$$P_0(\mu) = e^{-\omega\mu} = e^{-\mu_{vis}} \quad (2.15)$$

With N_{OR} the number of Fast-OR events in a given time interval, and N_{BCX} the corresponding number of bunch crossings, the probability to observe a Fast-OR P_{OR} in a given bunch crossing is:

$$P_{OR}(\mu) = \frac{N_{OR}}{N_{BCX}} = 1 - P_0(\mu) = 1 - e^{\mu_{vis}} \quad (2.16)$$

From the latter two one obtains an expression for μ_{vis} :

$$\mu_{vis} = -\ln(1 - P_{OR}(\mu)) \quad (2.17)$$

The PLT obtains μ_{vis} per telescope for each of the potential 3564 bunch positions for 4096 orbits of the LHC beam, also called nibble corresponding to 0.365 ms. Instead

of counting N_{OR} the fraction $f_0 = (1 - N_{OR}/N_{BCX})$ of no triple coincidences in that interval is measured. This has the advantage that the multiplicity of tracks does not have to be resolved and readout only has to register signal or no signal, 0 or 1, respectively. This is the digital mode and the method is called zero-counting. The mean number of tracks per collision is then given as $\mu_{vis} = -\ln(f_0)$. The μ_{vis} is summed over all bunch crossings and averaged over all telescopes and translated into the luminosity with the calibration constant σ_{vis} . Recently, instead of averaging over telescopes, the luminosity is provided on a per-telescope basis.

Chapter 3

Experimental Setup

This chapter describes the experimental facility used in the particle physics experiments. Section 3.1 covers the Large Hadron Collider (LHC), the accelerator complex responsible for delivering pp collisions to each experiment at CERN. Section 3.2 discusses the CMS detector. The Pixel Luminosity Telescope (PLT), the dedicated online luminometer for the CMS experiment is described in Section 3.3.

3.1 Large Hadron Collider

The Large Hadron Collider (LHC), first conceived in the 1980s, is the most powerful accelerator ever built with the aim of finding Higgs boson and search for particles and forces that interact between them not included in the SM. The collider is 27 kilometers in circumference and is placed 100 meters underground at the border between France of Switzerland near Geneva.

The LHC is the last step of a multi-stage chain of accelerators called the LHC accelerator complex as shown in Fig. 3.1. Hydrogen gas atoms are stripped off electrons and the remaining protons are accelerated in the 80 m long Linac 2 linear accelerator to a kinetic energy of 50 MeV. Protons then pass through three pre-accelerators Proton Synchotron Booster (PSB), Proton Synchotron (PS), and Super Proton Synchrotron (SPS) where they are accelerated to 1.4 GeV, 25 GeV, and 450

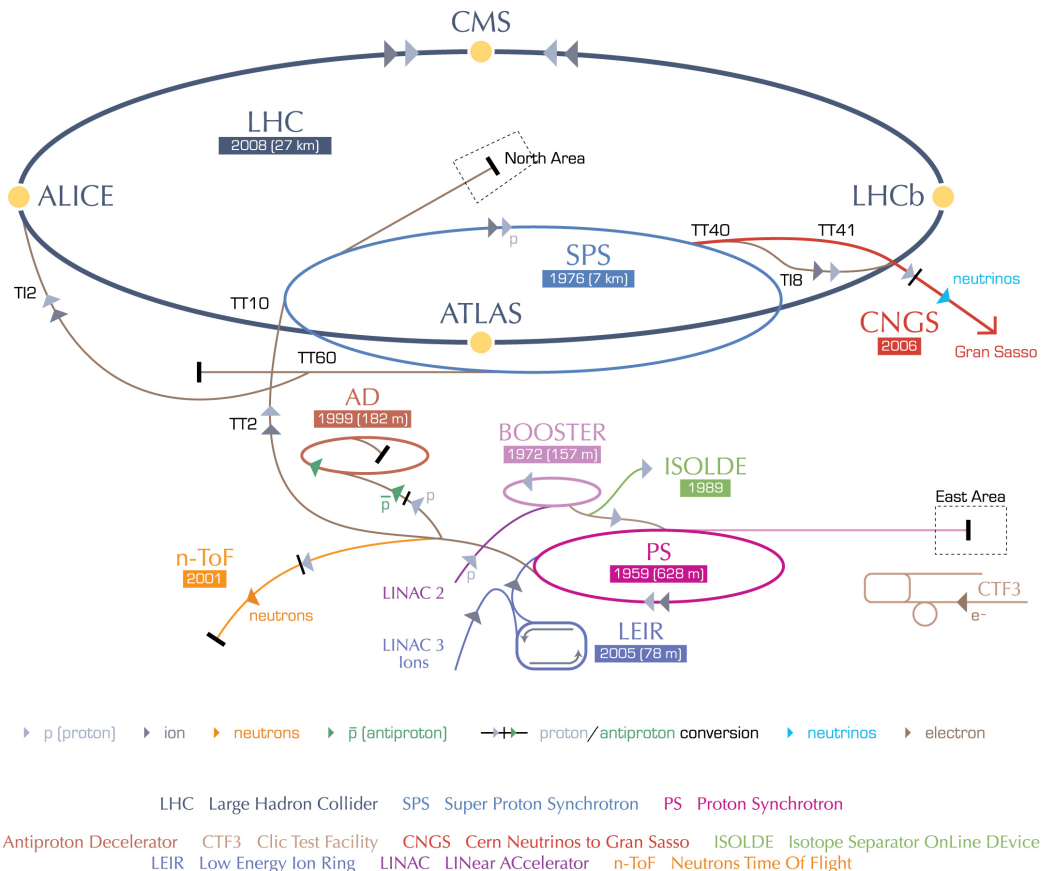


Figure 3.1: Layout of the CERN accelerator complex with four LHC experiments CMS, ALICE, ATLAS, and LHCb [Lefvre \(2008\)](#).

GeV, respectively. The proton beams are injected into the LHC ring where they are accelerated further to 6.5 TeV in opposite directions resulting a center-of-mass collision energy of 13 TeV.

Proton beams are segmented into groups of protons called bunches. Beams are kept on a circular path by 1232 dipole magnets located at various points around the ring. The magnetic field of 8.3 T operated at an ultracold temperature of 2 K (456 F) is generated by a superconducting coil cooled with liquid helium. Points 1, 2, 5, and 8 on the LHC ring are the interaction points where the beams overlap to produce collisions. Point 3 and 7 contain the beam collimation systems, and point 6 contains the beam dump system. The CMS experiment is located at interaction point 5.

3.1.1 Filling Scheme

Many protons are packed into each bunch to maximize the probability of a proton-proton collision for a given bunch crossing. Several filling patterns have been designed for various modes of operations of the LHC [Bailey and Collier \(2004\)](#). Typically, beams are arranged in the form of batches each with some continuous set of filled bunches.

The principle scheme for luminosity production is the 25 ns filling scheme, as shown in Figure 3.2, where each batch has 72 bunches totaling 2808 filled bunches. Gaps between the batches allow for the SPS and LHC fast injection magnets to change magnetic field, and the gap of 119 unfilled bunches at the end allows for the fast magnet that redirects the LHC beam into a beam dump to obtain full field strength. Each 25 ns bunch is confined to about 7.5 m out of the 27 km total distance in a given orbit.

3.1.2 LHC Operations in 2015 and 2016

The result described in this work is an analysis of the data taken with the Pixel Luminosity Detector for the CMS experiment during the operation of the LHC in

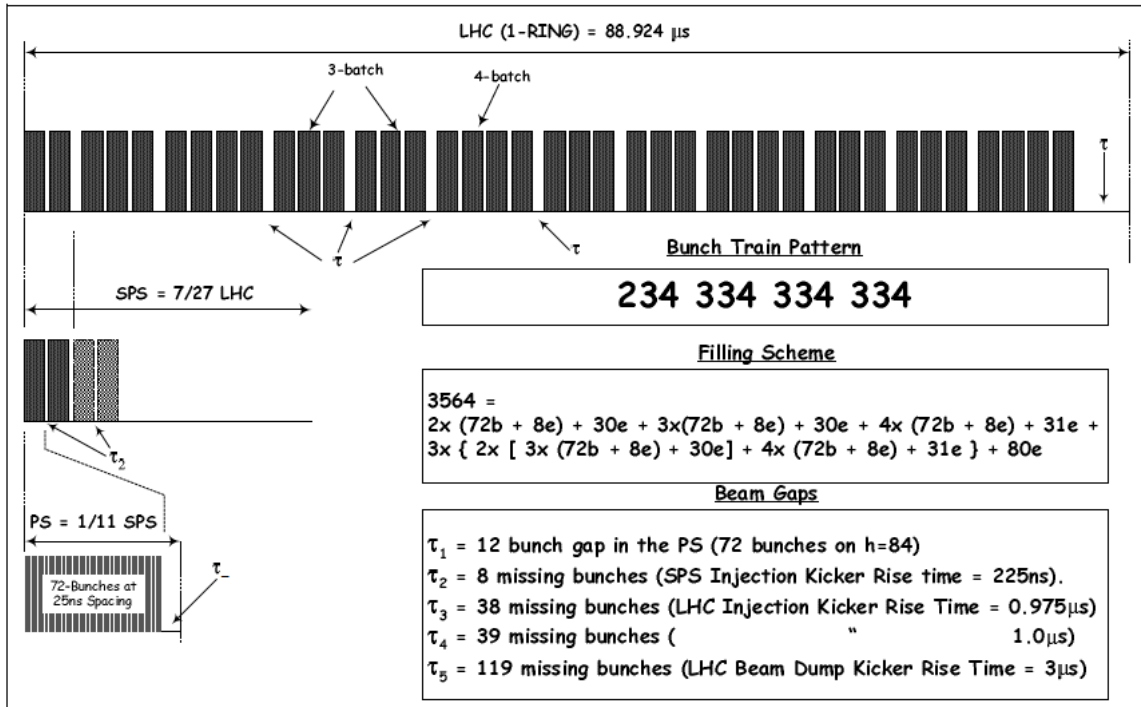


Figure 3.2: Schematic of the Bunch Disposition around an LHC Ring for the 25 ns Filling Scheme [Bailey and Collier \(2004\)](#). 'b' and 'e' indicate beam position with or without beam.

2015 and 2016. The center-of-mass energy of the pp collisions was 13 TeV. The average number of collision per bunch crossings, pileup, is shown in Figure 3.3 for this period.

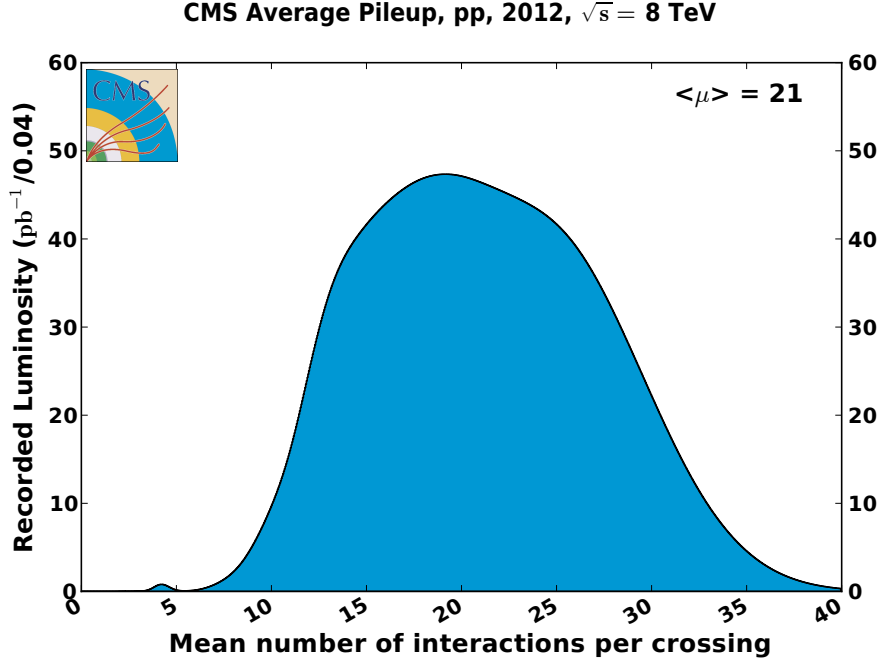


Figure 3.3: Mean number of interactions per bunch crossing, 2012.

3.2 CMS

Compact Muon Solenoid (CMS) is one of two general purpose particle-physics detectors on the LHC. It is designed to investigate a wide range of particles and phenomenon produced in the proton-proton collisions. The primary motivation for building this detector was to search for the Higgs boson and probe the standard model at energy scales above 1 TeV. This could shed some light into extensions of SM such as extra dimensions, supersymmetry , dark matter, and also gravity models around TeV scale.

The CMS coordinate system, as shown in Fig 3.4, is defined with the origin at the center of the detector. It is oriented such that the z -axis points along the LHC

ring in counterclockwise direction, x -axis towards the center of the LHC ring, and the y -axis vertically upwards above ground.

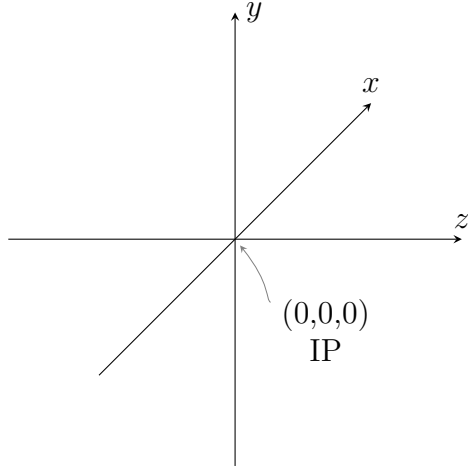


Figure 3.4: CMS Coordinate System with positive x towards the center of the ring

In the cylindrical coordinate system, r is the radius in the $x - y$ plane, ϕ the azimuthal angle in the $+x$ direction, and θ the polar angle in the $+z$ direction. The four momentum of a particle can be written as

$$p = \begin{pmatrix} E \\ \vec{p} \end{pmatrix}$$

where $\vec{p} = (p_x, p_y, p_z)$ in cartesian basis. The transverse momentum p_T in $r - \phi$ plane is given by

$$p_T = \sqrt{p_x^2 + p_y^2}$$

Particle kinematics can then be described by azimuthal angle, transverse momentum, and rapidity, y . Rapidity is additive under Lorentz transformations along the z axis and is given by

$$y = \frac{1}{2} \ln \left(\frac{E + p_z}{E - p_z} \right)$$

For relativistic particles the rapidity equals the pseudo-rapidity η , which is related to the particle polar coordinate by the following relation

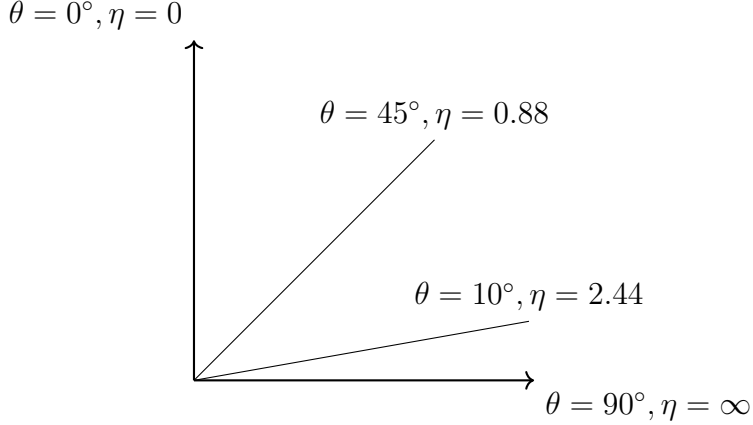


Figure 3.5: Relationship between polar angle and pseudorapidity.

$$\eta = -\ln(\tan(\theta/2))$$

The central feature of the CMS apparatus is a superconducting solenoid of 6 m internal diameter, providing a magnetic field of 3.8 T. Within the superconducting solenoid volume are a silicon pixel and strip tracker, a lead tungstate crystal electromagnetic calorimeter (ECAL), and a brass and scintillator hadron calorimeter (HCAL), each composed of a barrel and two endcap sections. Forward calorimeters extend the pseudorapidity [Collaboration \(2008\)](#) coverage provided by the barrel and endcap detectors. Muons are measured in gas-ionization detectors embedded in the steel flux-return yoke outside the solenoid.

Precise position measurement of charged particles coupled with strong magnetic field of the solenoid provides the parameters necessary for momentum resolution. The Electromagnetic Calorimeter and Hadronic Calorimeter provide the energy resolution. The Muon System and the silicon tracker measure the charged muon and inclusive particle positions respectively. The silicon tracker measures charged particles within the pseudorapidity range $|\eta| < 2.5$. It consists of 1440 silicon pixel and 15,148 silicon strip detector modules and is located in the 3.8 T field of the superconducting solenoid. For nonisolated particles of $1 < p_T < 10 \text{ GeV}$ and $|\eta| < 1.4$, the track resolutions are

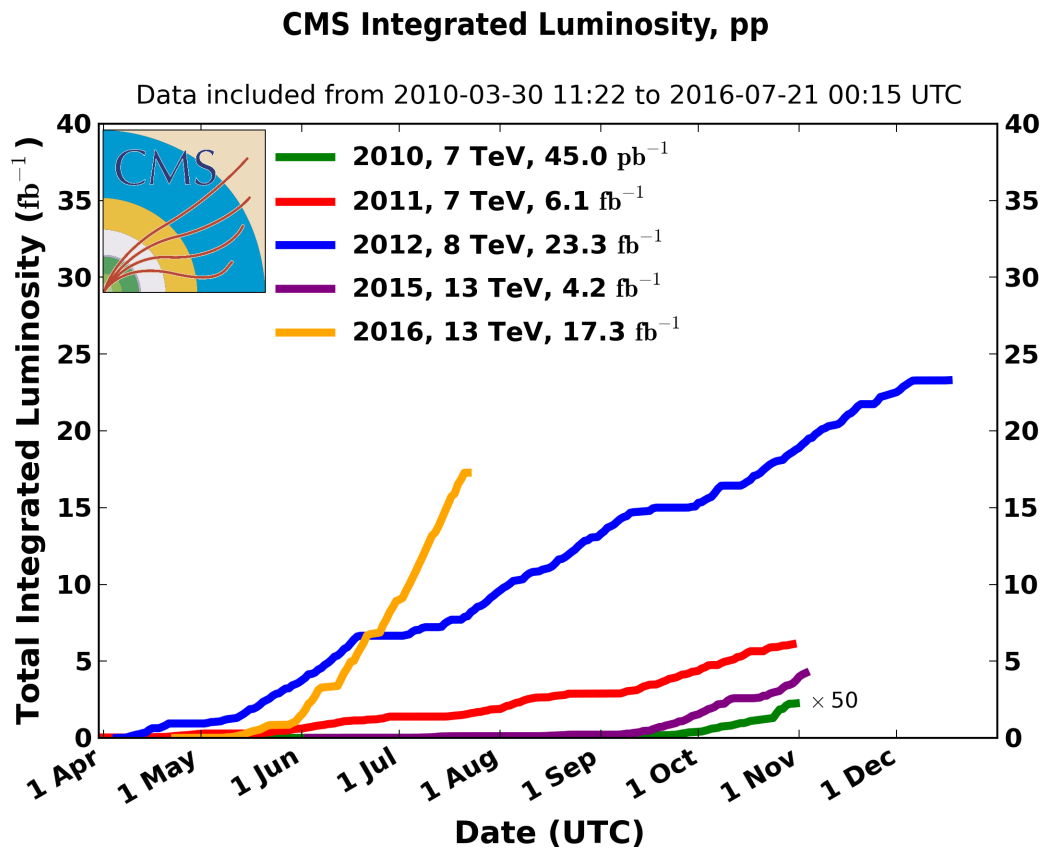


Figure 3.6: Delivered Luminosity versus time for several years of data taking of pp collisions with the CMS detector [CMS Collaboration \(2016\)](#).

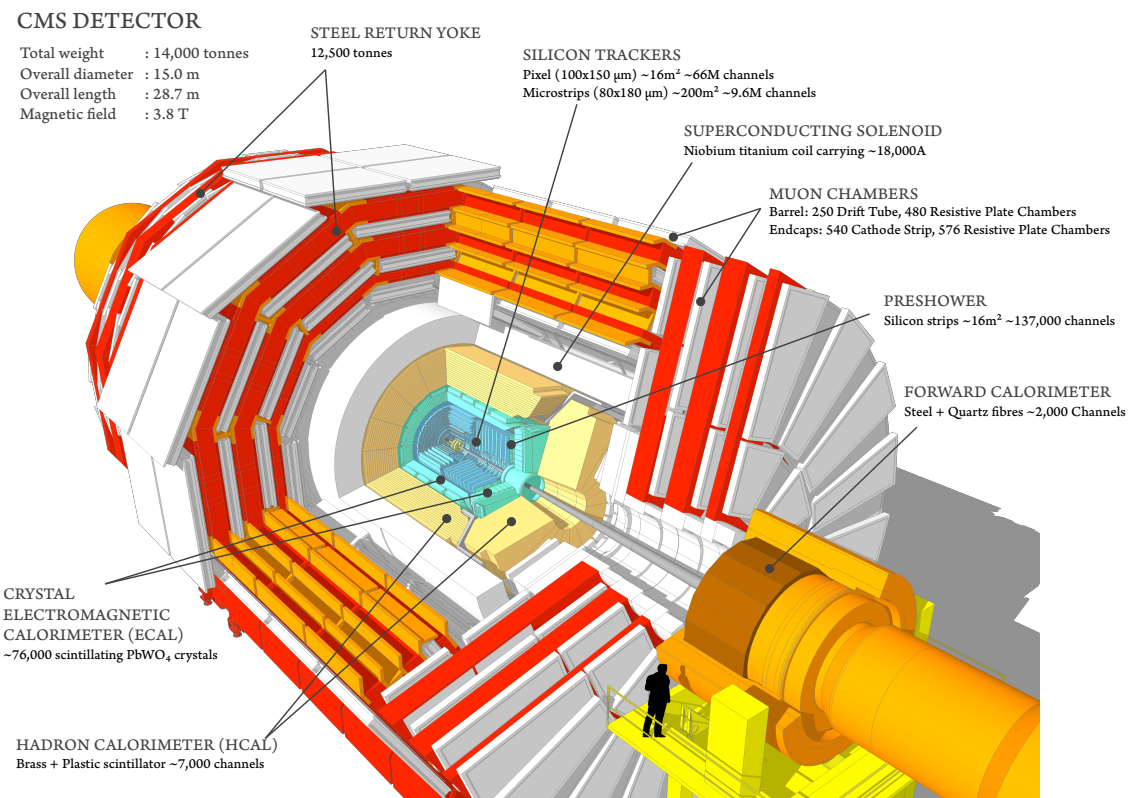


Figure 3.7: CMS Detector Sakuma (2016).

typically 1.5% in p_T and 25–90 (45–150) μm in the transverse (longitudinal) impact parameter Chatrchyan et al. (2014). A more detailed description of the CMS detector, together with a definition of the coordinate system used and the relevant kinematic variables, can be found in Ref. Collaboration (2008).

3.3 Pixel Luminosity Telescope

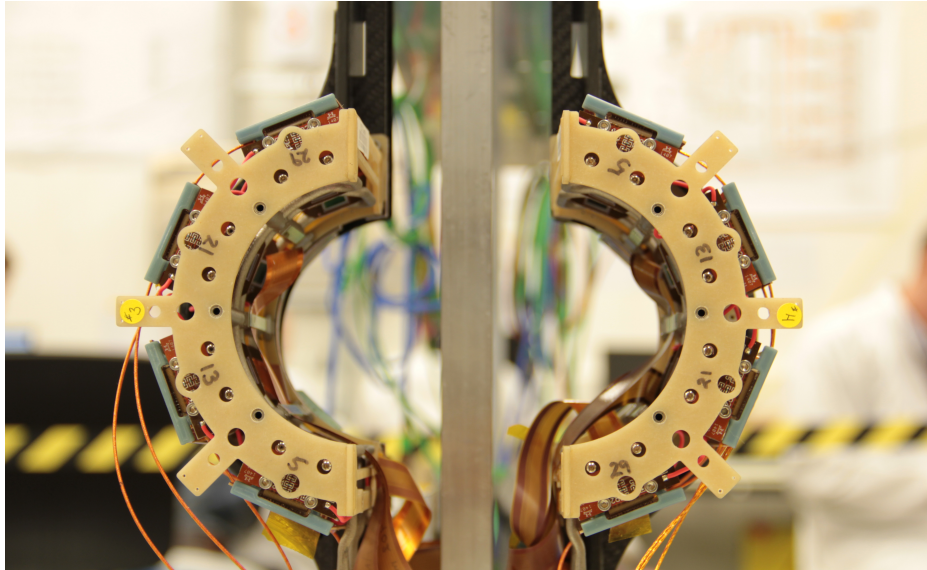


Figure 3.8: PLT Module.

The Pixel Luminosity Telescope is a dedicated system for measuring the luminosity at CMS using silicon pixel sensors Kornmayer (2015). The instrument is positioned close to the beam pipe and directly behind the Forward Pixel detector. It is located at a pseudo rapidity, $|\eta|$, of roughly 4 and at a mean radial distance of ~ 5 cm from the beam. It was installed in January 2015 as part of the Run 2 upgrades for the CMS Beam Radiation Instrumentation and Luminosity (BRIL) project Dabrowski (2014), and has operated successfully throughout the 2015 and 2016 run of the LHC.

The PLT consists of a forward and backward module with each having 8 telescopes. Each telescope consists of 3 consecutive planes of silicon pixel detectors spaced apart by 3.75 cm. Each pixel sensor is segmented into 80 rows and 52 columns of pixels,

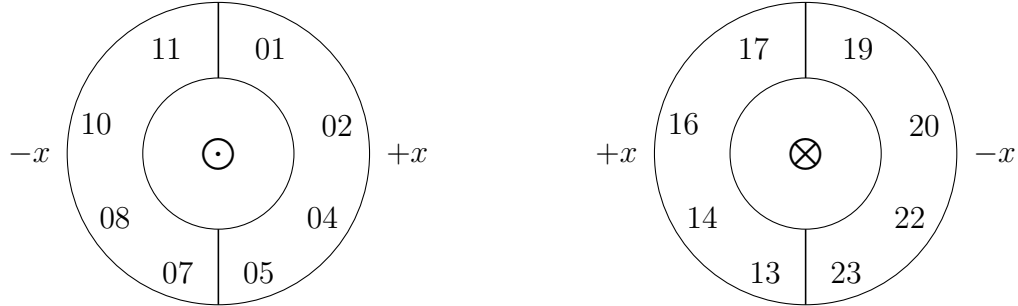


Figure 3.9: PLT modules at forward direction(left) and backward direction (right) both located at 171 cm from the interaction point.

with each pixel $150 \mu\text{m}$ wide and $100 \mu\text{m}$ high for a total active area of about $8 \times 8 \text{ mm}^2$. The middle plane is placed 0.102 cm higher than the first plane, and the third plane is placed 0.102 cm higher than the middle plane to maintain an average viewing angle of 0.27 degrees toward the interaction point.

Read Out Chip (ROC)

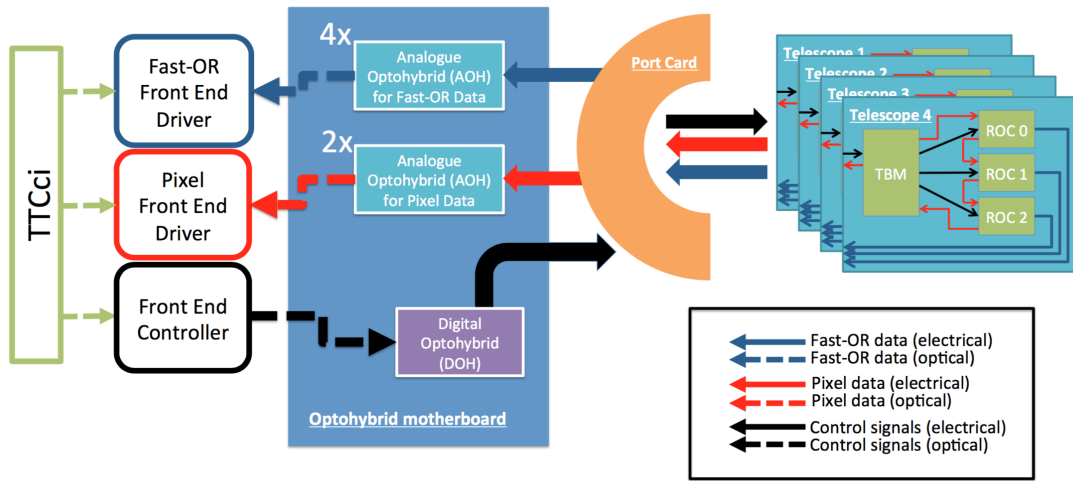


Figure 3.10: A schematic of the control and readout logic of Pixel Luminosity Telescope.

The sensors are read out by a PSI46v2 readout chip (ROC), the same that is used in the CMS pixel detector Kästli et al. (2006); Gabathuler (2005); Barbero (2003).

Each ROCs from each telescopes are connected to a HDI card, which contains the Token Bit Manager (TBM) chip that handles the readout of the series of ROCs [Bartz \(2005\)](#). A port card, which manages the communication and control signals, is connected to half of the telescopes in each side which is then connected to opto-motherboard which converts the electrical signals into optical signals. The four telescopes connected to a single port card are identified by their hub number, which are (in clockwise order) 5, 13, 21, and 29 as shown in Appendix Table. ?? and ??.

Data Streams

The front-end readout electronics consist of a FEC (Front-End Controller) card, which issues commands to the ROCs [Allkofer et al. \(2008\)](#), and three FED (Front-End Driver) cards [Pernicka et al. \(2007\)](#). One FED is responsible for the readout of the pixel data from the ROCs , and is identical to the FEDs used by the pixel detector. The other two FEDs (one for each side of the detector) read out the Fast-OR data from the ROCs.

The pixel data [Barbero \(2003\)](#) is read out via Slink and saved to disk on a dedicated computer hard drive, while the Fast-OR data is collected in a histogram with the FED. The histogram contains a bin for each bunch crossing (BX) and is incremented by 1 in case a telescope found at least 1 signal count for each sensors. The counts within the bins are added for every 4096 orbits (lumi nibble) corresponding to a time interval of about 13. ms. The integration occurs via a VME PC which is connected to the FED via a optical bridge.

Fast-OR Data

The 52 columns in a sensor is segmented into a group of double columns, 0-26. Each hit on a double column is registered as a signal. For a given bunch crossing, the hits in double columns per sensor are reported to the FED which tests if there was at least one signal in each of the three planes. This triple-coincidence count rate is translated to luminosity value as described in sec [3.3.2](#).

Pixel Data

Each pixel of a sensor is calibrated beforehand where some amount of charge collected can be translated to some number of hits. Once a sensor registers a charge signal above some threshold value, the pulse height and pixel address together with the timestamp information is saved to a buffer. Once the pixel detector receives a valid external signal trigger, the information is transferred to the FED via optical connections.

Trigger

The rate of collision, proportional to LHC bunch crossings of 25 ns, translates to a frequency of 40 MHz. A trigger is used to reduce the amount the data to a more manageable rate. To this end, two different approaches were employed: a trigger generated by taking an OR of the fast-or coincidence signals from all of the channels was used in the early 2015 run to maximize the pixel data taken. It means that if any of the channels registered a triple coincidence for a BX, FED looked for hit signals for that BX. Starting late 2015, a purely random trigger at a rate of 2 kHz was used to avoid any systematic uncertainties in the trigger that could have been introduced by our choice of using fast-or signals for trigger signals.

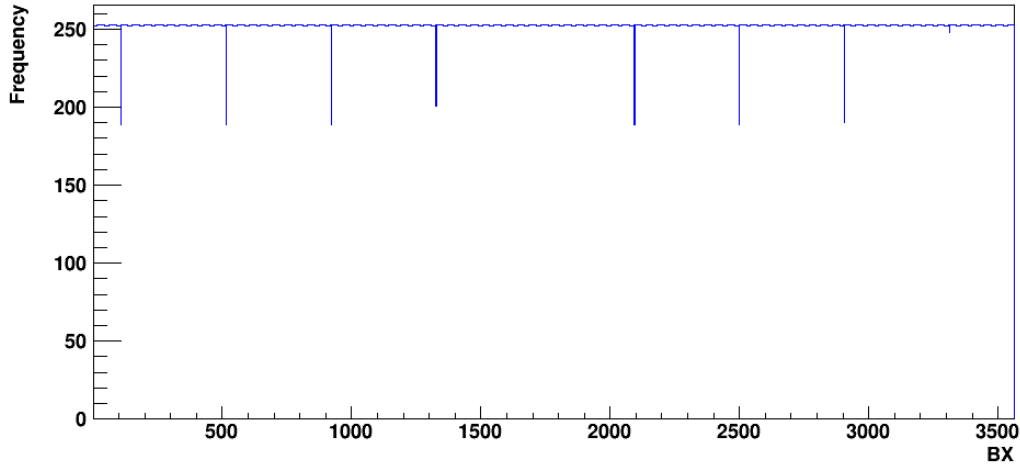


Figure 3.11: Bunches triggered via random trigger setup for ~ 10 lumi sections from Fill 5151 (2016) with 1579 BX cycling every 3 orbits

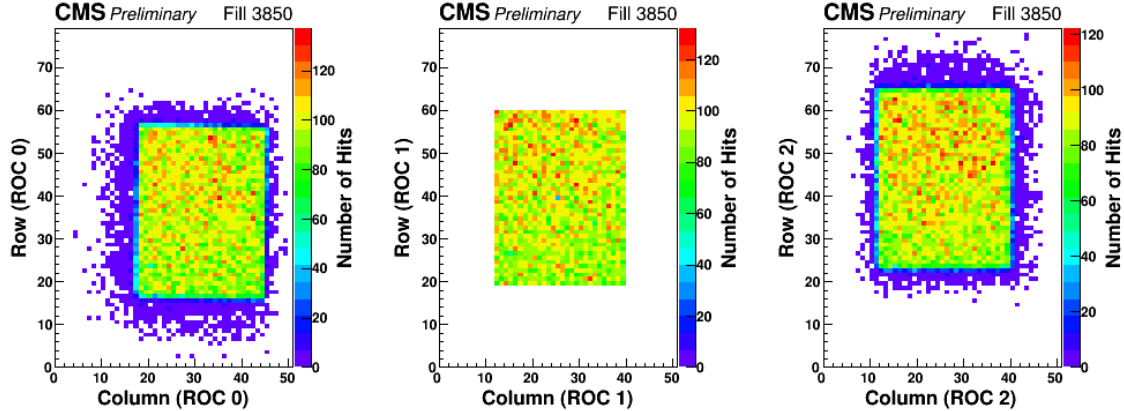


Figure 3.12: Tracks which make through all 3 planes with a mask of 4mm x 4mm

TTCCi hardware supports internal random trigger or a fixed sequence of intervals [TTCCi User Guide \(2007\)](#). In order to achieve a sufficiently random trigger within 3564 bins and achieve a manageable rate of 3 kHz, trigger is made to advance by 1585 bunches every 3 orbits (out of 4096 per nibble). Fig. 3.11 shows the BXes triggered via random trigger setup for the Fill 4444 from September 30, 2015. One downside of having a random trigger approach is that pixel data gets saved at high rate even when there is no beam.

3.3.1 Triple coincidence measurement

Real tracks are assumed to hit all three planes in a given telescope. In other words, the magnetic field has little effect on the trajectory of particles hitting the telescopes. The fast-or data is saved in a histogram where each bin is separated by 25 ns bunch spacing. Each bin of the histogram records the number all the triple coincidences on all three planes for each telescope over a 1 lumi-nibble which is 4096 orbits.

Figure 3.12 shows the occupancies in a single telescope of the Pixel Luminosity Telescope (PLT) with a mask applied to reduce the active area of the central plane to 4mm x 4mm. This plot shows only events where a triple coincidence (a simultaneous hit in all three planes) occurred in this specific telescope, allowing us to measure the effects of alignment and accidentals.

In order to decrease the contribution from combinatoric effects producing fake triple coincidences, the active area of the sensors was decreased by masking out outer pixels. The center plane in each telescope was reduced to an active area of 4.2x4.0 mm (28 columns x 40 rows) and the outer two planes to 5.4x5.2 mm (36 columns x 52 rows).

During early commissioning operations, Channels 22 and 23 in Fig. 3.9, stopped responding and were dropped from the luminosity calculations. One more telescope, Channel 1 also was taking out of the calculation in 2016 data taking period.

3.3.2 Zero Counting Algorithm

The average occupancy of the PLT at the LHC design luminosity is about 0.1 per BX. For a given telescope, the number of hits that it receives in a bunch crossing can be considered a simple counting experiment. Figure 3.13 shows the mean number of coincidence count per telescope for a sample data.

The number of hits is proportional to the length of the interval, which is 25ns in our case. The probability of occurrence of two or more hits is very small and the number of events for one bin is independent of what happens in another bin. As such, the triple-coincidence count can be treated as a problem in Poission statistics as described in sec 2.4.

3.3.3 Van der Meer Scan Calibration

The Van der Meer (VdM) scans procedure [Van Der Meer \(1968\)](#) is used to measure the conversion factor between the number of tracks measured by the PLT and the delivered luminosity as described in 2.3. The LHC performed the VdM procedure for CMS on 24th August 2015 (LHC Fill 4266), and on 27th May 2016 (LHC Fill 4954)

The relationship between the instantaneous luminosity provided by the LHC and the mean number of tracks per bunch crossing, μ_{tracks} , is given by

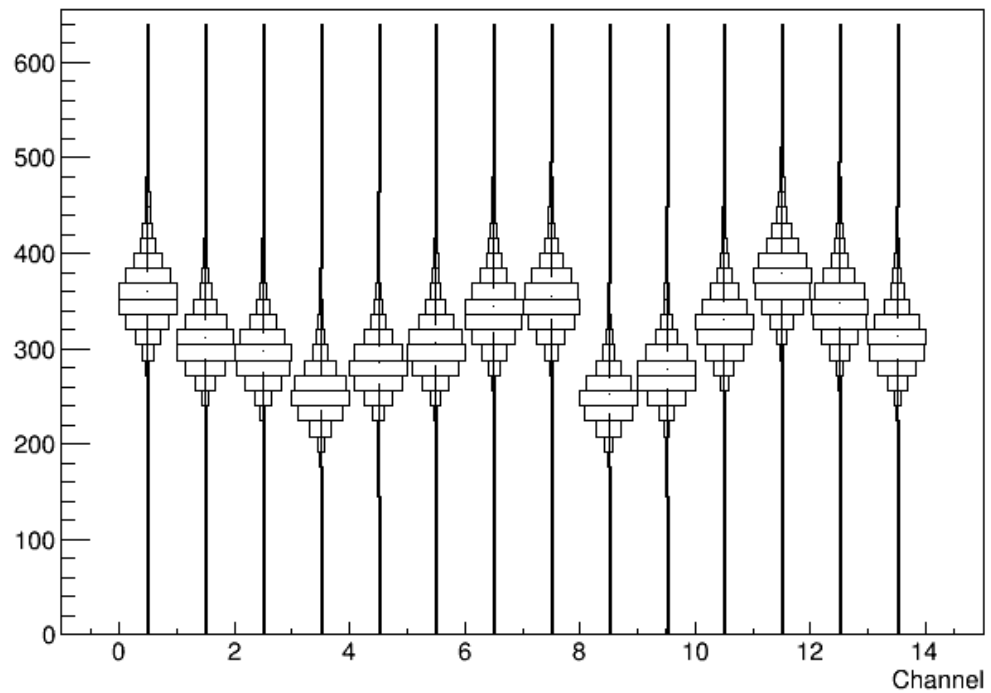


Figure 3.13: Per channel average coincidence count for 1 nibble sample from Fill 4444 (2015)

$$\frac{dL}{dt} = \frac{\mu_{tracks} f}{\sigma_{vis}}$$

Where f is the LHC revolution frequency of 11,246 Hz and σ_{vis} is the fraction of the total inelastic cross-section of CMS visible to the PLT. One can then determine σ_{vis} via the VdM procedure, as described in section 2.3 and 2.4, using only the LHC beam parameters as follows:

$$\frac{dL}{dt} = \frac{I_1 I_2 f}{2\pi\sigma_x\sigma_y}$$

Here, I_1 and I_2 are the measured beam currents, and σ_x and σ_y are the beam width parameters along the x and y axes. The LHC Fast Bunch Current Transformers (FBCT) and beam Quality Monitoring (BQM) independently provide bunch-to-bunch measurement of beam currents. The measured current over bunches is then normalized to the total current by the Dirct-Current Current Transformers (DCCT). Figure 3.14 shows a comparison of the luminosity measurement via LHC parameters and Pixel Luminosity Detector for the CMS experiment [Lujan et al. \(2016\)](#).

σ_x and σ_y are derived from fits of the observed number of PLT Fast-OR as a function of the beam separation. For each of the five scan pairs, the beams are moved between $+6\sigma$ and -6σ in steps of 0.5σ . Each fit can then be performed on the resulting 25 data points. As the beam has been found to be non-Gaussian to a degree, the fit is performed using a combination double-Gaussian function

$$R(\Delta_{x/y}) = a_1 \exp\left\{ \frac{-(\Delta_{x/y} - \mu)^2}{2\sigma_1^2} \right\} + a_2 \exp\left\{ \frac{-(\Delta_{x/y} - \mu)^2}{2\sigma_2^2} \right\}$$

where the means of each Gaussian are constrained to be equal, and the effective constant a_{eff} and effective width σ_{eff} are given by:

$$a_{eff} = a_1 + a_2$$

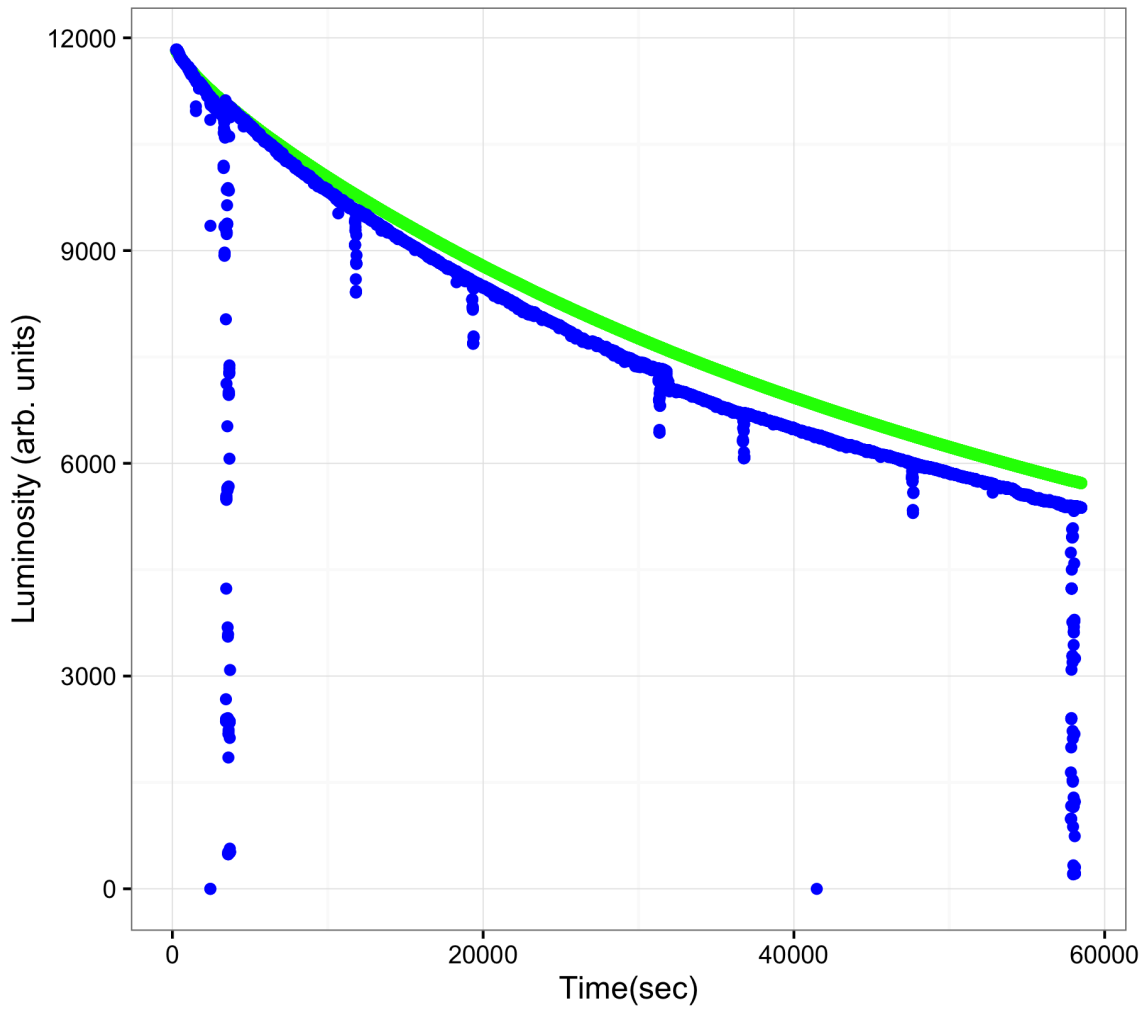


Figure 3.14: Comparison of luminosity measured via LHC beam parameters and Pixel Luminosity Detector for the CMS experiment, Fill 5253.

$$\sigma_{eff} = \frac{a_1\sigma_1 + a_2\sigma_2}{a_1 + a_2}.$$

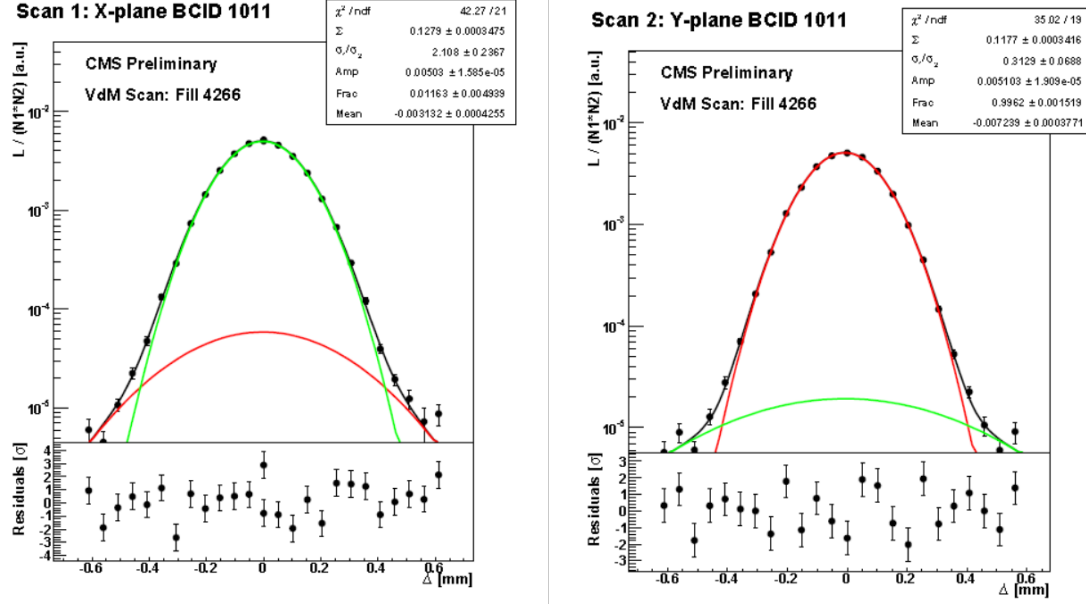


Figure 3.15: Double Gaussian fit to PLT track rate as a function of beam separation, for bunch 1011 during the first separation/crossing VdM scan in X and Y.

The final conversion factors extracted via the vdm scan for 2015 and 2016 are blah1 and blah2 respectively with a relative uncertainty of ...%.

Bibliography

Bibliography

- Allkofer, Y. et al. (2008). Design and performance of the silicon sensors for the CMS barrel pixel detector. *Nucl. Instrum. Meth.*, A584:25–41. [26](#)
- Bailey, R. and Collier, P. (2004). Standard filling schemes for the various LHC operation modes. *LHC Project Note 323*. [ix](#), [x](#), [8](#), [17](#), [18](#)
- Barbero, M. (2003). *Development of a radiation-hard pixel read out chip with trigger capability*. PhD thesis, Basel U., Basel. <https://cds.cern.ch/record/467141>. [25](#), [26](#)
- Bartz, E. (2005). The $0.25\mu\text{m}$ token bit manager chip for the CMS pixel readout. In *11th Workshop on Electronics for LHC and Future Experiments*. CERN. CERN-2005-011. [26](#)
- Chatrchyan, S. et al. (2014). Description and performance of track and primary-vertex reconstruction with the CMS tracker. *JINST*, 9:P10009. [24](#)
- CMS Collaboration (2016). CMS luminosity public results. <https://twiki.cern.ch/twiki/bin/view/CMSPublic/LumiPublicResults>. [x](#), [22](#)
- Collaboration, C. (2008). The CMS experiment at the CERN LHC. *JINST*, 3:S08004. [21](#), [24](#)
- Dabrowski, A. (2014). Upgrade of the CMS instrumentation for luminosity and machine induced background measurements. Technical Report CMS-CR-2014-362, CERN, Geneva. [24](#)

- Gabathuler, K. (2005). Psi46 pixel chip - external specification. <http://cmspixel.phys.ethz.ch/docs/psi46-readout-chip/psi46v2.pdf>. 25
- Herr, W. and Muratori, B. (2003). Concept of luminosity. *proceedings of CERN Accelerator School*. 8
- Kästli, H. C., Barbero, M., Erdmann, W., Hormann, C., Horisberger, R., Kotlinski, D., and Meier, B. (2006). Design and performance of the CMS pixel detector readout chip. *Nucl. Instrum. Meth.*, A565:188–194. 25
- Kornmayer, A. (2015). The CMS pixel luminosity telescope. *Nucl. Instrum. Meth. A*. 24
- Lefvre, C. (2008). The CERN accelerator complex. Complexe des accélérateurs du CERN. x, 16
- Lujan, P., Riley, G., Rose, K., Spanier, S., and Thapa, K. (2016). PLT luminosity measurement, corrections, and systematic uncertainty for the 2015 run. CMS Analysis Note CMS-AN-2016/002, BRIL PLT. 12, 31
- Pernicka, M., Kotlinski, D., Johns, W., Steininger, H., and Schmid, H. (2007). The CMS Pixel FED. 26
- Sakuma, T. (2016). 3d sketchup images of the cms detector (120918). CMS Document 11514-v3. x, 23
- TTCci User Guide (2007). <http://cmsdoc.cern.ch/cms/TRIDAS/ttc/modules/ttcci/>. Accessed: 09-26-2016. 28
- User:MissMJ, N. et al. (2014). Standard model of elementary particles. http://commons.wikimedia.org/wiki/File:Standard_Model_of_Elementary_Particles_modified_version.svg. x, 4
- Van Der Meer, S. (1968). Calibration of the effective beam height in the ISR. Technical Report CERN-ISR-PO-68-31. ISR-PO-68-31, CERN, Geneva. 10, 29

White, S. M., Burkhardt, H., and Puzo, P. (2010). *Determination of the Absolute Luminosity at the LHC*. PhD thesis, Orsay, Universit Paris-Sud 11, Orsay.
Presented on 11 Oct 2010. [11](#)

Appendix

Appendix A

Summary of Equations

A.1 Cartesian

some equations here

A.2 Cylindrical

some equations also here

Vita

Vita goes here...